



PROJECT: Pyrolysis of Wood

CL316: Separation Process - II

Gaurav Budhwani

2211085

Chemical Engineering

Kaushik

22110113

Chemical Engineering

Professor

Karthik Subramaniam Pushpavanam

April 28, 2025

Contents

1	Introduction	1
2	Objectives	2
3	Modeling and Theory	2
3.1	Heat Transfer	2
3.2	Mass Transport	3
3.3	Chemical Reactions	3
3.4	Coupled Physics	4
4	Experimental Setup	4
5	Parameter Estimation	5
6	Results	6
6.1	Varying Radius of Wood Particle	6
6.2	Varying Porosity of Wood Particles	13
6.3	Varying Reaction Kinetics (Pre-Exponential Factors and Activation Energies)	18
6.4	Effect of Varying Ambient Temperature	22
7	Parameter Estimation and Optimisaton	25
7.1	Analysis of Results	25
7.2	Key Improvements via Parameter Estimation	36
7.3	Comparison of Initial and Optimized Parameters	37
8	Conclusion	38

Abstract

This project investigates the pyrolysis of a wood particle under inert conditions using COMSOL Multiphysics. A coupled heat transfer, species transport, and chemical reaction model was developed, and parametric studies were conducted varying porosity, reaction kinetics, and ambient temperature. Furthermore, a detailed parameter estimation procedure was employed to fit the model outputs to experimental temperature and mass loss data. Optimized parameters yielded significant improvements in predictive accuracy, closely matching experimental trends. The results highlight the importance of heat and mass transfer properties in pyrolysis and demonstrate that calibrated models can reliably simulate biomass decomposition. Future work includes extending the model to incorporate more detailed kinetics and radiative heat transfer.

1 Introduction

Pyrolysis is a process where materials are broken down by heating them without any oxygen present. When wood is heated in this way, it decomposes into three main products: gas, tar (which includes water and oily substances), and a solid material called charcoal. This technique has been used since ancient times to produce important materials like tar for waterproofing ships and charcoal for metal smelting. Even today, pyrolysis remains an important process because it allows us to create useful fuels and chemicals from renewable biomass like wood, instead of depending on fossil fuels.

In the past, wood pyrolysis was done by covering burning wood with dirt to stop air from entering, letting it smolder slowly. In modern times, pyrolysis is performed in closed reactors where nitrogen or other inert gases are used to prevent oxygen from reaching the wood. The products and how much of each is formed depend heavily on factors such as the type of wood, the size of the particles, the heating rate, the final temperature, and how long the process is run.

Modeling the pyrolysis process helps scientists and engineers predict how wood behaves when heated. Because the chemical reactions inside wood are extremely complex, we use simplified models that group the different products into a few categories, called "lumped species." In this project, the model divides the products into gas, tar, an intermediate solid, and charcoal. This makes it easier to study how wood breaks down over time.

The model also considers that wood is not uniform. It behaves differently along the direction of the wood fibers compared to across them. To capture this, the model treats heat and mass transfer as being anisotropic, meaning properties like thermal conductivity and permeability vary with direction.

In the experiment behind this model, a small sphere of wood (about 1 cm in diameter) is heated in a furnace at constant temperature with nitrogen gas flowing around it. Thermocouples are placed at the surface, middle, and center of the sample to measure temperatures as the wood heats up and decomposes. The weight of the wood is also recorded to track how much mass is lost during pyrolysis.

Finally, parameter estimation is used to improve the model. Initially, the model uses guessed values for certain parameters like reaction rates and heat transfer coefficients. Parameter estimation adjusts these guesses by comparing the model's predictions to the real experimental results. By doing this, the model becomes more accurate and reliable for predicting how wood will behave under different pyrolysis conditions.

Applications of Pyrolysis Modeling Pyrolysis modeling has practical relevance in designing biomass reactors, optimizing biochar production, and renewable energy systems [2, 3]. Accurately predicting thermal degradation of wood enables improved control of yields and efficiency in thermochemical processes. Thus, reliable simulations are crucial for advancing sustainable energy

technologies.

2 Objectives

The objectives of this project are:

- To model the pyrolysis of wood under inert atmospheric conditions using COMSOL Multiphysics.
- To simulate heat transfer, mass transport, and chemical reactions during the pyrolysis process.
- To implement a lumped reaction scheme involving gas, tar, intermediate solid, and char.
- To perform parameter estimation by fitting the model predictions to experimental data.
- To validate the model by comparing simulated results with the experimental mass loss and temperature profiles.

3 Modeling and Theory

The pyrolysis of wood involves several physical processes occurring simultaneously, including heat transfer, chemical reactions, gas movement, and mass loss. To accurately describe these, the model combines different physical principles into one coupled simulation.

3.1 Heat Transfer

Heat must first travel into the wood particle to initiate decomposition. Because wood heats unevenly, the surface reaches higher temperatures before the center. Additionally, wood has different thermal properties along the fiber direction compared to across it, a behavior known as anisotropic heat transfer.

In the model:

- Heat is conducted within the solid material.
- Convection occurs as gases move through the porous structure.
- Radiative heat transfer also takes place inside the pores.
- At the surface, heat loss to the surrounding gas is modeled through convection and radiation.

The energy balance accounts for the heating of the material and the energy absorbed or released during chemical reactions, which can be either endothermic or exothermic.

3.2 Mass Transport

As the wood decomposes, gases and vapors are generated inside the particle. These species move through the pores and escape, causing a decrease in the solid mass.

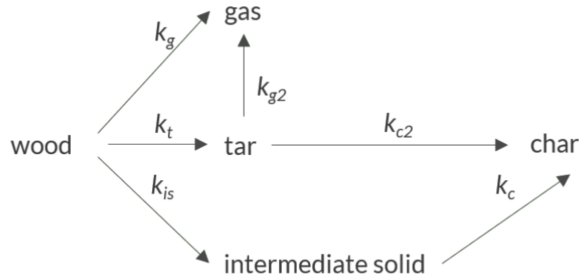
The model captures:

- Diffusion of gases inside the particle, modeled using Fick's law.
- Pressure-driven gas flow, described by Darcy's law.
- Convective mass transfer at the external boundary, assuming no diffusive resistance.

The porosity of the material increases over time as solid wood is converted into gaseous products, creating additional pathways for mass transport.

3.3 Chemical Reactions

The complex reactions occurring during pyrolysis are simplified into a lumped reaction scheme:



- Primary reactions convert wood into gas, tar, and an intermediate solid.
- Secondary reactions decompose tar into gas or char.
- The intermediate solid ultimately converts into char.

Each reaction rate follows an Arrhenius-type expression:

$$k = A \exp\left(\frac{-E}{RT}\right)$$

where k is the reaction rate constant, A is the frequency factor, E is the activation energy, R is the gas constant, and T is the temperature.

3.4 Coupled Physics

All the physical processes are strongly coupled:

- Heat influences the rate of chemical reactions.
- Reactions produce gases that affect flow and heat transport.
- Gas movement carries away heat and chemical species.

Therefore, the model simultaneously solves the equations for heat transfer, mass transport, and chemical kinetics, updating the temperature, pressure, gas concentrations, and solid composition at every time step.

4 Experimental Setup

The pyrolysis experiment was performed using an isothermal furnace under an inert atmosphere, with continuous monitoring of the sample mass and internal temperatures.

A small wooden sphere, approximately 1 cm in radius, was placed inside the furnace. The furnace temperature was kept constant throughout the experiment, and a steady flow of nitrogen gas was maintained to ensure that pyrolysis occurred without combustion.

The sample was mounted on a holder connected to a sensitive scale positioned outside the furnace. This arrangement allowed continuous measurement of the sample mass as pyrolysis progressed, capturing the mass loss due to the release of gases and tars.

Three thermocouples were inserted into the wood sample to monitor the temperature profile at different locations:

- One thermocouple at the surface,
- One thermocouple at the midpoint (halfway between the center and surface),
- One thermocouple at the center.

These thermocouples measured the internal temperatures at different depths, which is crucial for understanding the heat penetration and reaction rates inside the particle.

The overall setup is illustrated in Figure 1.

The experimental data collected include the time-dependent temperature at the surface, midpoint, and center, as well as the normalized mass of the sample. These measurements were used to validate the simulation and perform parameter estimation.

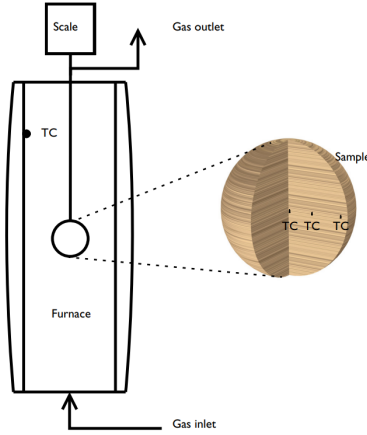


Figure 1: The experimental system setup consists of an isothermal furnace with inert atmosphere, a sample holder attached to a scale, and thermocouples (TC) measuring the temperature of the sample at different positions. The sample radius is approximately 1 cm.

5 Parameter Estimation

Parameter estimation is an important step in improving the accuracy of the simulation model. In pyrolysis modeling, many parameters such as reaction rates, heats of reaction, and heat transfer coefficients are not exactly known beforehand and may vary depending on the material and experimental conditions.

In this project, parameter estimation was performed to match the model predictions with the experimental data more closely. The goal was to minimize the difference between the simulated and measured values of:

- Sample mass loss over time,
- Temperature profiles at the surface, midpoint, and center of the sample.

The parameters selected for estimation were:

- The Arrhenius frequency factor (A_{is}) for the primary pyrolysis reaction,
- The heat of reaction for the formation of tar (ΔH_t),
- The heat of reaction for the formation of char (ΔH_c),
- The external convective heat transfer coefficient (h_{conv}).

The parameter estimation was formulated as a nonlinear least-squares optimization problem. The objective is to minimize the sum of squared differences between the model predictions and the experimental data:

$$q_{\text{opt}} = \arg \min_q \sum_{n=1}^N Q_n \quad (1)$$

where the term Q_n for each experiment is defined as:

$$Q_n = \frac{1}{2} \sum_{m=1}^{M_n} \left(P_n(u(q), q) - \hat{P}_{nm} \right)^2 \quad (2)$$

Here:

- q is the vector of control parameters to be estimated,
- $P_n(u(q), q)$ is the model prediction at data point m for experiment n ,
- \hat{P}_{nm} is the corresponding experimental measurement,
- M_n is the number of data points in experiment n ,
- N is the total number of experiments considered.

The optimization process adjusts the selected parameters until the model output (temperature and mass loss) best fits the experimental data. This improves the reliability and predictive capability of the simulation.

6 Results

The simulation results for the pyrolysis of wood were obtained by solving the coupled heat transfer, mass transport, and chemical reaction models using COMSOL Multiphysics. Both initial and parameter-estimated simulations were performed. Key phenomena such as pressure buildup, volatile transport, temperature evolution, and decomposition behavior were analyzed. Detailed insights are presented below for the effect of particle radius, porosity, and reaction kinetics.

6.1 Varying Radius of Wood Particle

The particle radius was varied across four cases: 0.01 m, 0.1 m (base), 0.5 m, and 1.0 m. This analysis highlights how size impacts internal pressure gradients, velocity fields, decomposition extent, volatile release, and thermal distribution.

Surface Pressure and Darcy's Velocity Field

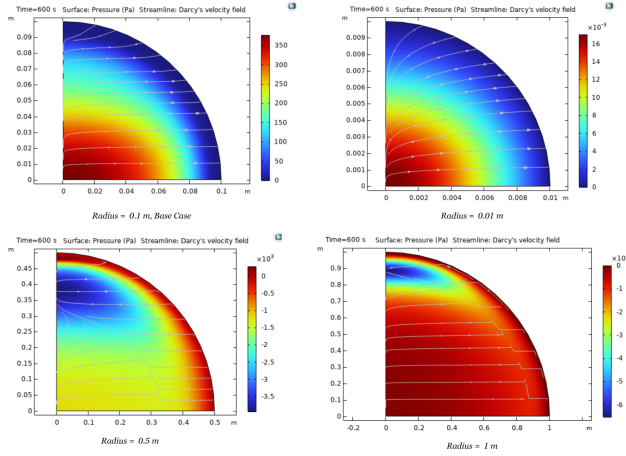


Figure 2: Surface pressure (Pa) and Darcy velocity streamlines for different particle radii at 600 seconds during pyrolysis.

Analysis: Figure 2 illustrates the pressure distribution and gas flow within particles of different sizes. In the smallest particle (0.01 m), the pressure remains relatively low and uniform, with rapid gas escape indicated by dense streamlines. As particle size increases:

- Significant negative pressures develop near the surface, reaching about -3500 Pa for the 0.5 m particle and -6000 Pa for the 1.0 m particle.
- Velocity streamlines become more sparse inside larger particles but are concentrated near the surface, indicating slower internal flow but stronger surface venting.
- Larger particles experience higher internal gas generation but lower permeability-driven flow, leading to pressure accumulation.

This behavior is governed by Darcy's law:

$$\mathbf{u} = -\frac{\kappa}{\mu} \nabla p$$

where larger ∇p is needed to drive gas through longer diffusion paths in big particles.

Conclusion: Larger particles trap volatiles longer, creating stronger outward pressure gradients and delayed gas release compared to small particles.

Wood Density Distribution

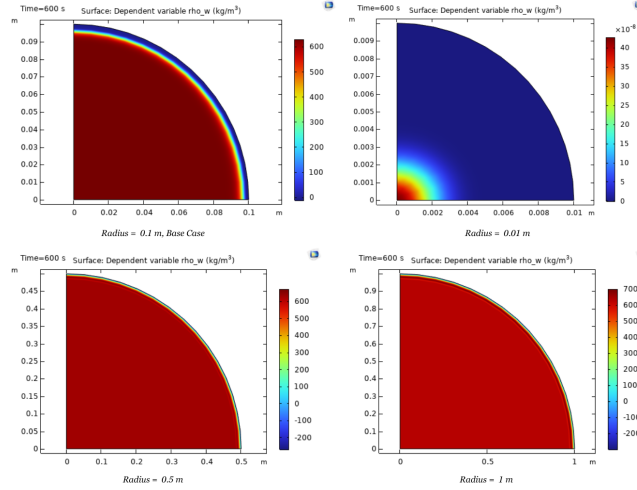


Figure 3: Wood density (ρ_w , kg/m^3) distribution across different particle radii at 600 seconds.

Analysis: Figure 3 shows that:

- The 0.01 m particle is nearly uniformly decomposed, with $\rho_w \approx 0$ across most of the volume.
- The 0.1 m particle shows significant depletion near the surface but retains higher density ($600 \text{ kg}/\text{m}^3$) at the core.
- The 0.5 m and 1.0 m particles maintain high core density ($>700 \text{ kg}/\text{m}^3$), with decomposition only at outer layers.

The solid density decreases from surface inward, indicating that pyrolysis is primarily a heat- and mass-transfer-limited process.

Conclusion: Small particles decompose uniformly due to fast heat penetration, while large particles exhibit "shrinking-core" behavior where only surface layers pyrolyze initially.

Surface Molar Concentration and Flux of Tar Species

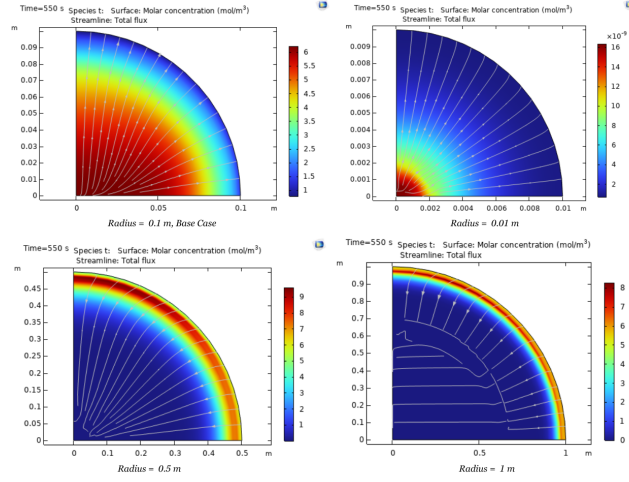


Figure 4: Surface molar concentration (mol/m^3) and total flux of tar species at 550 seconds for different radii.

Analysis: Figure 4 reveals that:

- For the 0.01 m particle, tar concentration near the surface rapidly drops, indicating fast generation and escape.
- In the 0.5 m and 1.0 m cases, tar accumulates within the core (up to $9 \text{ mol}/\text{m}^3$), with slower outward diffusion.
- Flux vectors are denser and stronger for smaller particles, signifying higher tar migration rates.

Conclusion: Smaller particles favor efficient tar evolution and release; larger particles exhibit tar buildup due to slower diffusion and delayed pyrolysis.

Surface Molar Concentration and Flux of Gas Species

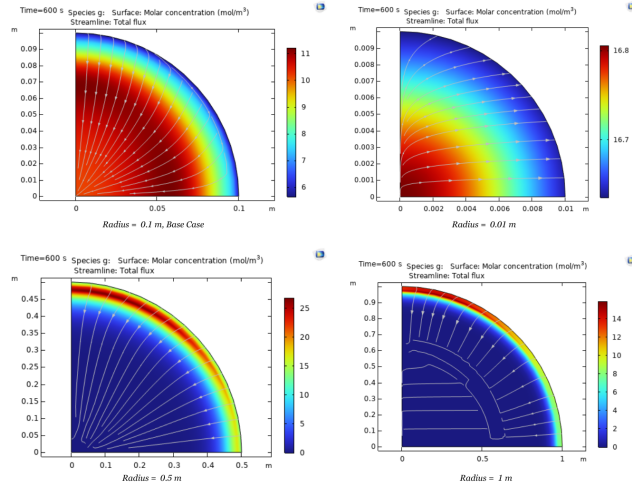


Figure 5: Surface molar concentration and total flux of gas species at 600 seconds for different particle radii.

Analysis: From Figure 5:

- Small particles (0.01 m) exhibit relatively uniform gas concentrations ($6\text{--}11 \text{ mol}/\text{m}^3$) and strong surface flux.
- Large particles retain much higher core concentrations ($20 \text{ mol}/\text{m}^3$), with weak and uneven flux distribution.

This confirms that gas species are generated but trapped in large particles, while smaller ones facilitate faster venting.

Conclusion: Gas generation and transport are size-dependent, with larger particles hindering gas migration and causing buildup.

Surface Molar Concentration and Flux of Nitrogen Species

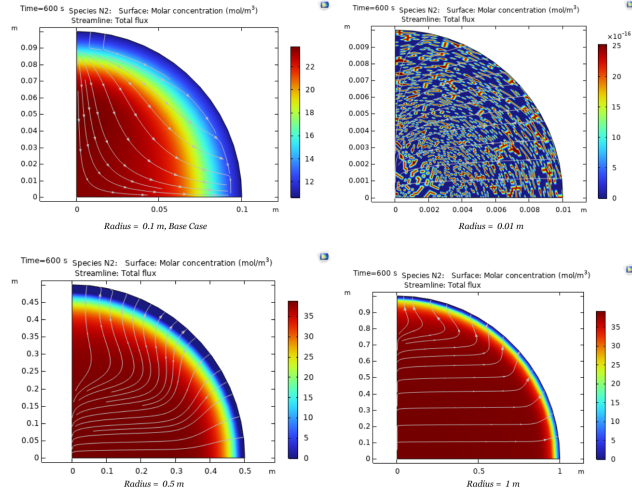


Figure 6: Surface molar concentration and total flux of nitrogen (N_2) at 600 seconds for different radii.

Analysis: As seen in Figure 6:

- Nitrogen, being inert, exhibits minimal core-to-surface gradients.
- In small particles, slightly faster flushing of N_2 is observed due to greater permeability and shorter diffusion lengths.

No significant reaction-driven changes occur for N_2 species.

Conclusion: Nitrogen serves as an indicator of gas flow dynamics but is otherwise unaffected by the pyrolysis chemistry.

Temperature Distribution and Isothermal Contours

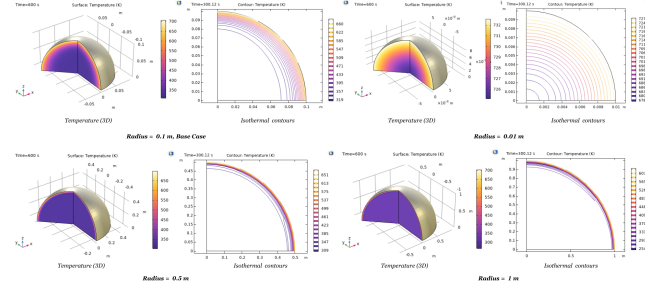


Figure 7: Temperature distribution (K) and isothermal contours during pyrolysis for different particle radii at 600 seconds.

Analysis: Figure 7 shows:

- Small particles (0.01 m) achieve relatively uniform heating (350–732 K).
- Large particles (1.0 m) have cooler cores (309 K) and only partial surface heating (663 K).
- Strong radial temperature gradients exist for large sizes, slowing reaction rates per Arrhenius law:

$$k = A \exp \left(-\frac{E}{RT} \right)$$

Thermal diffusion controls pyrolysis progression: smaller particles heat uniformly and react faster; larger particles remain thermally stratified with delayed decomposition.

6.2 Varying Porosity of Wood Particles

Surface Pressure and Darcy's Velocity Field

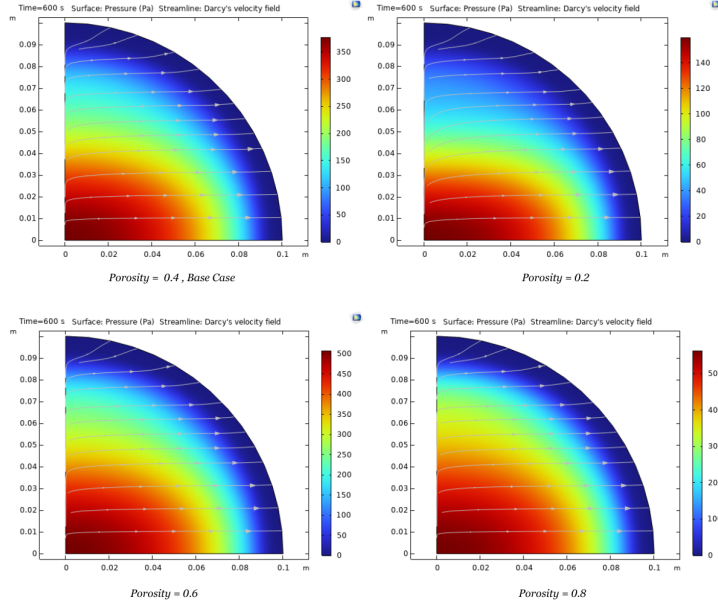


Figure 8: Surface Pressure and Darcy's Velocity Field for Different Porosities at 600 seconds

Analysis: The figure shows the distribution of pressure (Pa) and gas velocity streamlines inside a wood particle (radius 0.1 m) at varying porosities: 0.2, 0.4 (base case), 0.6, and 0.8. As porosity increases:

- **Porosity 0.2:** Low surface pressure (140 Pa) and sparse velocity streamlines suggest restricted gas flow due to limited permeability.
- **Porosity 0.4:** Moderate surface pressure (350 Pa) with visible streamlines. Represents balanced gas movement.
- **Porosity 0.6:** Peak surface pressure (450 Pa) and denser streamlines, indicating enhanced gas release.
- **Porosity 0.8:** Surface pressure slightly reduces (300 Pa), but velocity streamlines are densest, showing free and rapid gas escape.

Conclusion: Increasing porosity enhances gas mobility and volatile release. However, pressure buildup does not linearly increase: extremely high porosity (0.8) lowers pressure due to rapid gas venting, even though velocity is high. This suggests an optimal porosity for maximizing both pressure-driven and diffusion-driven flows.

Wood Density Distribution

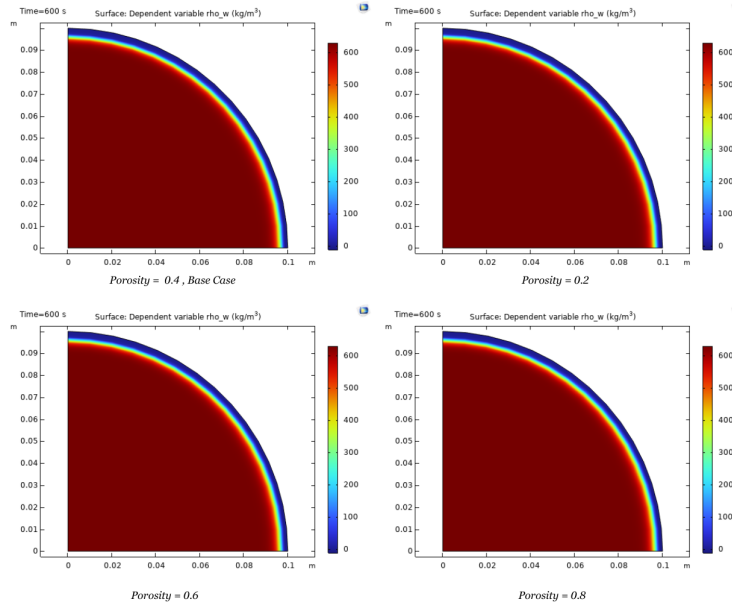


Figure 9: Wood Density (ρ_w) Distribution at Different Porosities at 600 seconds

Analysis: The figure captures the degradation of wood density (ρ_w , kg/m^3) within the particle.

- **Porosity 0.2:** Core density remains high ($600 \text{ kg}/\text{m}^3$), indicating minimal decomposition.
- **Porosity 0.4:** Notable reduction in surface density; core still dense but shows transition.
- **Porosity 0.6:** Larger surface layer with reduced density ($0 \text{ kg}/\text{m}^3$) showing more extensive pyrolysis.
- **Porosity 0.8:** Broadest low-density region, with deep penetration of decomposition toward the core.

Conclusion: Higher porosity allows faster removal of volatiles, promoting deeper reaction fronts. Lower porosity delays volatile escape, slowing the pyrolysis progress.

Molar Concentration and Flux of Tar Species

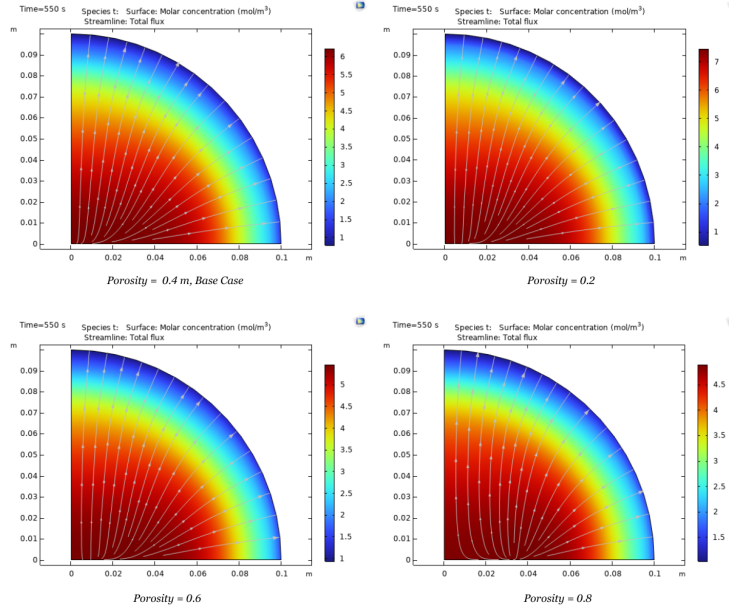


Figure 10: Molar Concentration and Total Flux of Tar Species at Different Porosities at 550 seconds

Analysis: The concentration and flux of tar species (t) evolve distinctly:

- **Porosity 0.2:** High tar accumulation in the core ($7 \text{ mol}/\text{m}^3$), poor flux.
- **Porosity 0.4:** Moderate tar reduction near the surface.
- **Porosity 0.6:** Better surface depletion ($1 \text{ mol}/\text{m}^3$), indicating tar escape.
- **Porosity 0.8:** Strong tar flux and lowest core concentration ($4.5 \text{ mol}/\text{m}^3$), highlighting superior tar transport.

Conclusion: High porosity accelerates tar removal, while low porosity leads to tar trapping and delayed decomposition. Flux patterns corroborate this behavior.

Molar Concentration and Flux of Gas Species

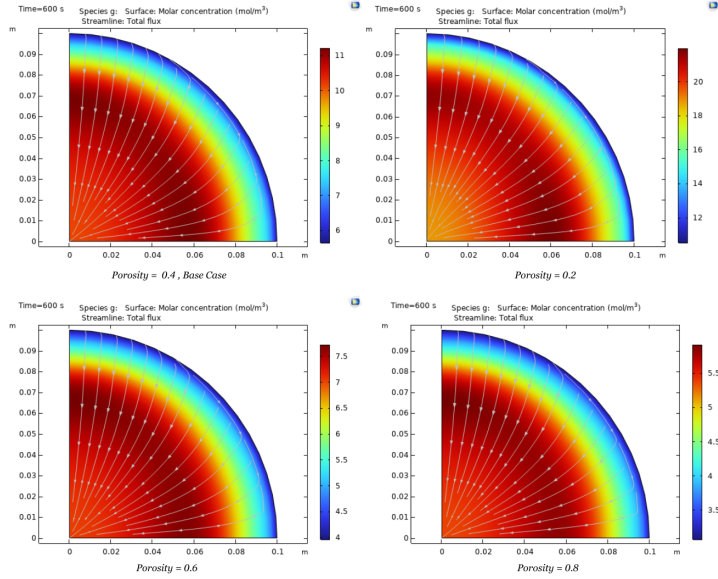


Figure 11: Molar Concentration and Total Flux of Gas Species at Different Porosities at 600 seconds

Analysis: For gas species (g):

- **Porosity 0.2:** Severe gas accumulation (20 mol/m³ in the core) and weak outward flux.
- **Porosity 0.4:** Smoother gas migration.
- **Porosity 0.6 and 0.8:** Significant gas release with lower concentration gradients.

Conclusion: Gas movement mirrors tar behavior: higher porosity reduces internal resistance, thus promoting faster gas removal and reducing buildup.

Molar Concentration and Flux of Nitrogen Species (N_2)

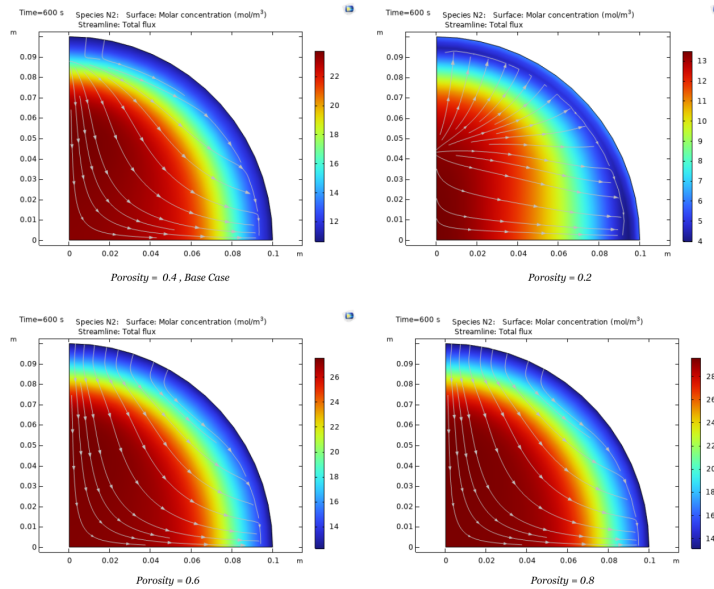


Figure 12: Molar Concentration and Total Flux of Nitrogen (N_2) at Different Porosities at 600 seconds

Analysis: Nitrogen, being inert, tracks gas flow:

- **Porosity 0.2:** High core concentration ($13 \text{ mol}/\text{m}^3$), sluggish flux.
- **Porosity 0.6 and 0.8:** Lower core concentration, denser flux streamlines.

Conclusion: Higher porosity enhances nitrogen transport, confirming overall improvement in fluid dynamics with porosity.

Temperature Distribution and Isothermal Contours

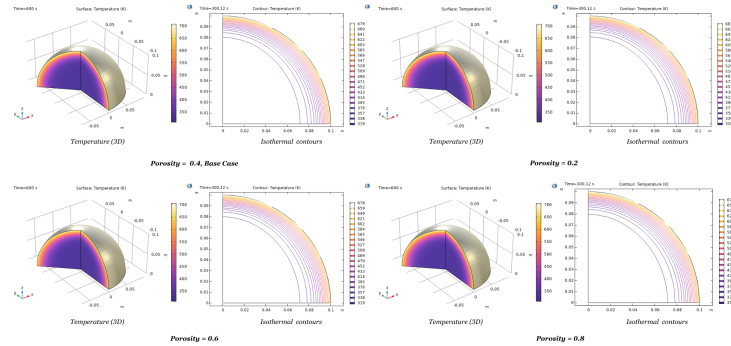


Figure 13: Temperature Distribution and Isothermal Contours at Different Porosities at 600 seconds

Analysis: Thermal profiles reveal:

- **Porosity 0.2:** Strong thermal gradients; surface 679 K while core 319 K.
- **Porosity 0.4:** Intermediate gradient (350–700 K).
- **Porosity 0.6 and 0.8:** More uniform heating across the particle.

Conclusion: Higher porosity not only promotes volatile release but also facilitates better heat penetration, leading to faster and more uniform pyrolysis.

6.3 Varying Reaction Kinetics (Pre-Exponential Factors and Activation Energies)

Surface Pressure and Darcy's Velocity Field

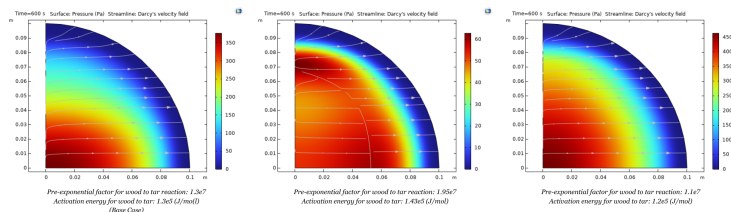


Figure 14: Surface Pressure and Darcy's Velocity Field for Different Reaction Kinetics at 600 seconds

Analysis: The figure shows how altering the reaction kinetics (specifically, increasing activation energy) affects internal pressure and gas flow:

- **Base Case ($E_a = 1365 \text{ J/mol}$):** Moderate surface pressure (350 Pa) with strong and dense velocity streamlines indicating rapid volatile generation and escape.
- **Higher $E_a = 19567 \text{ J/mol}$:** Reduced surface pressure (300 Pa), sparse streamlines, suggesting slowed volatile formation and weaker flow.
- **Intermediate $E_a = 14265 \text{ J/mol}$:** Higher surface pressure (450 Pa), denser streamlines than the highest activation energy case but lower compared to base case.

Conclusion: Higher activation energy slows down reaction rates, reducing volatile generation, and thereby suppressing pressure buildup and Darcy velocity.

Wood Density Distribution

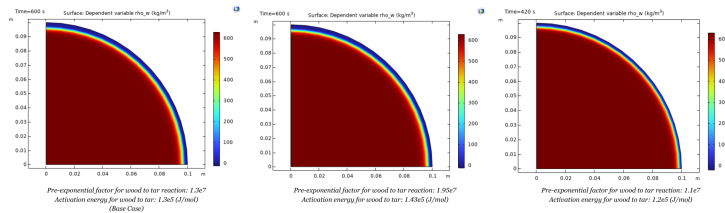


Figure 15: Wood Density (ρ_w) Distribution for Different Reaction Kinetics

Analysis: The extent of pyrolysis (density reduction) varies strongly with kinetics:

- **Base Case:** Near-complete surface decomposition (surface $\rho_w \approx 0$) by 600 s.
- **19567 J/mol:** Substantial residual core density (600 kg/m³) with only a narrow surface layer showing decomposition.
- **14265 J/mol at 424 s:** Moderate density reduction compared to 19567 J/mol case, but still much slower than the base case.

Conclusion: Higher activation energies significantly delay wood decomposition. The base case kinetics allow faster reaction progression and mass loss.

Molar Concentration and Flux of Tar Species

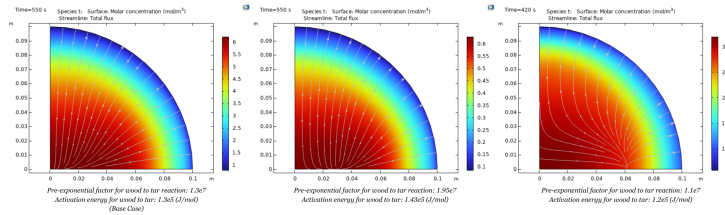


Figure 16: Molar Concentration and Total Flux of Tar Species for Different Reaction Kinetics

Analysis: Tar species behavior varies with kinetics:

- **Base Case:** Strong surface tar depletion (to $1.5 \text{ mol}/\text{m}^3$) and dense flux streamlines indicating vigorous tar release.
- **14365 J/mol:** Higher residual core tar concentration ($5.5 \text{ mol}/\text{m}^3$), less tar flux.
- **14265 J/mol at 424 s:** Delayed tar generation, moderate flux, indicating slowed pyrolysis.

Conclusion: Higher activation energy suppresses tar production and transport, delaying and reducing the volatile output compared to lower E_a cases.

Molar Concentration and Flux of Gas Species

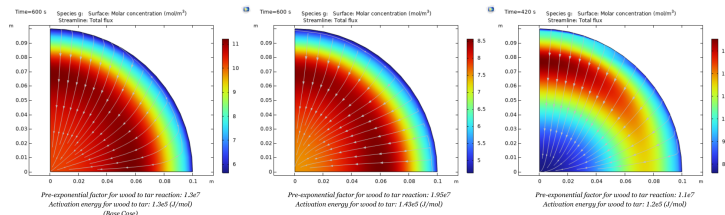


Figure 17: Molar Concentration and Total Flux of Gas Species for Different Reaction Kinetics

Analysis: The evolution of gas species follows a similar trend:

- **Base Case:** Core concentration reduces to $6 \text{ mol}/\text{m}^3$, with strong flux indicating active gas release.
- **14365 J/mol:** Higher core concentration ($8.5 \text{ mol}/\text{m}^3$), weaker surface flux.

- **14265 J/mol at 424 s:** Even greater core gas retention (13 mol/m³), implying strongly delayed pyrolysis.

Conclusion: Gas production and release slow down as activation energy increases, corroborating the suppressed pyrolysis rates.

Molar Concentration and Flux of Nitrogen Species (N₂)

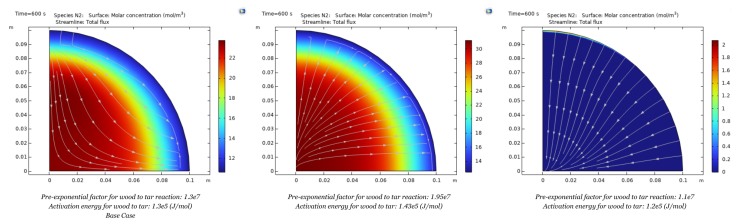


Figure 18: Molar Concentration and Total Flux of Nitrogen (N₂) for Different Reaction Kinetics

Analysis: Nitrogen movement patterns also reflect the kinetic influence:

- **Base Case:** Rapid nitrogen evacuation from the core (22 mol/m³ to 12 mol/m³ surface).
- **14365 J/mol:** Core concentration increases (30 mol/m³), reduced flux.
- **14265 J/mol:** Severe suppression of nitrogen migration; near-complete core retention.

Conclusion: Reduced reaction rates (higher E_a) slow down nitrogen clearing, although nitrogen itself is non-reactive. It highlights slower bulk fluid movement.

Temperature Distribution and Isothermal Contours

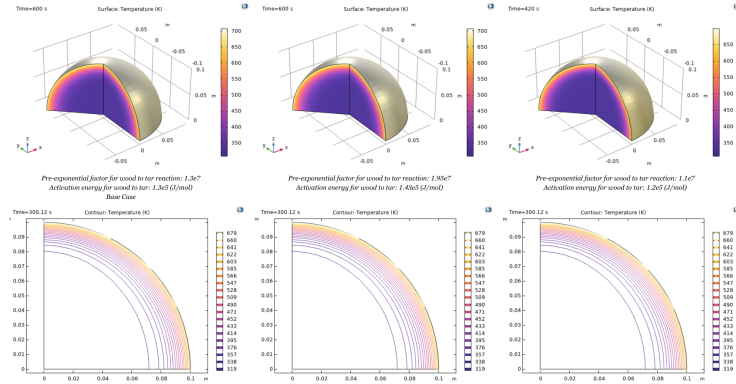


Figure 19: Temperature Distribution and Isothermal Contours for Different Reaction Kinetics

Analysis: Temperature evolution changes markedly with kinetics:

- **Base Case:** Smooth temperature profile, surface temperatures reaching 700 K at 600 s.
- **14365 J/mol:** Slower heating, surface 679 K, tighter thermal gradients.
- **14265 J/mol at 424 s:** Surface temperatures much lower (600 K), large cold core zones.

Conclusion: Higher activation energy not only delays pyrolysis chemistry but also indirectly slows temperature rise because endothermic reactions (absorbing heat) progress slower.

6.4 Effect of Varying Ambient Temperature

In this section, the ambient (furnace) temperature surrounding the wood particle is varied to study its impact on the pyrolysis process. Different ambient temperatures modify the heat flux into the particle, affecting internal pressure, volatile species generation, mass loss, and temperature profiles.

Surface Pressure and Darcy's Velocity Field

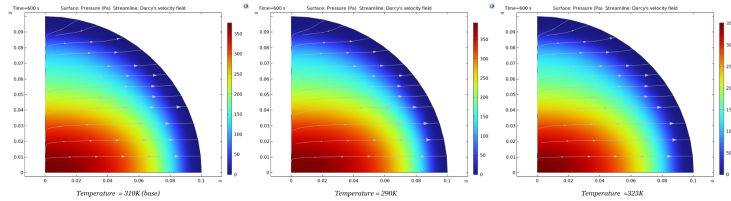


Figure 20: Surface Pressure and Darcy's Velocity Field at 600 Seconds Under Varying Ambient Temperatures

Analysis: As the ambient temperature increases from 290 K to 328 K:

- At 290 K: Lower surface pressure (300 Pa), sparse streamlines, indicating reduced gas movement.
- At 310 K (Base): Moderate surface pressure (350 Pa) and balanced gas flow.
- At 328 K: Higher surface pressure (450 Pa), densest streamlines, enhanced gas release.

Conclusion: Higher ambient temperatures significantly increase internal pressure and gas velocity, promoting faster volatile release. The base temperature (310 K) provides optimal flow without excessive venting.

Molar Concentration and Flux of Tar Species

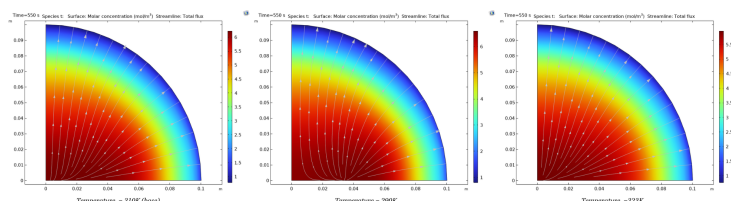


Figure 21: Molar Concentration and Flux of Tar Species at 550 Seconds Under Varying Ambient Temperatures

Analysis: Higher ambient temperatures enhance tar production and migration:

- 328 K shows steep concentration gradients and the densest flux lines.
- 310 K provides balanced tar production and flux.
- 290 K results in reduced tar release due to limited heating.

Conclusion: Raising the ambient temperature increases tar yield and flux, while cooling retards tar generation and migration.

Molar Concentration and Flux of Gas Species

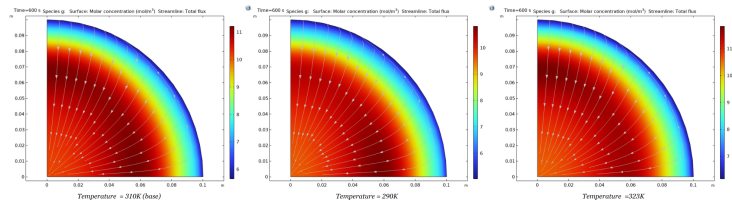


Figure 22: Molar Concentration and Flux of Gas Species at 600 Seconds Under Varying Ambient Temperatures

Analysis: Similar behavior as tar:

- At 328 K: Maximum gas flux.
- At 310 K: Moderate flux.
- At 290 K: Minimum gas flux and higher retention inside the particle.

Conclusion: Higher temperatures facilitate faster gas production and outward migration, enhancing pyrolysis efficiency.

Molar Concentration and Flux of N₂ Species

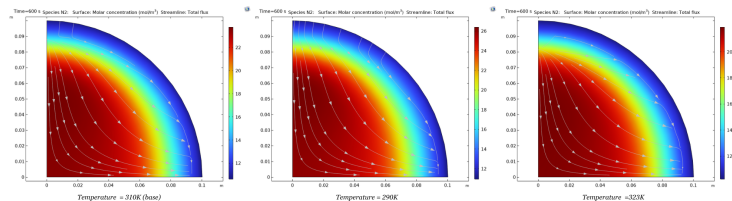


Figure 23: Molar Concentration and Flux of Nitrogen (N₂) Species at 600 Seconds Under Varying Ambient Temperatures

Analysis: N₂ transport mirrors that of reactive species:

- Faster outward flux at higher temperatures.
- Slower evacuation at 290 K.

Conclusion: Inert N₂ serves as an indicator of overall gas flow; higher ambient temperature increases the efficiency of gas transport.

7 Parameter Estimation and Optimisaton

Parameter estimation is the process of adjusting model parameters (such as reaction rate constants, activation energies, heat of reaction, and heat transfer coefficients) so that the simulation outputs closely match experimental measurements. It is critical because initial guesses often lead to significant discrepancies between simulation and real-world behavior.

One of the important metrics used in this process is the normalized mass (Y), defined as:

$$Y(t) = \frac{m(t)}{m_0}$$

where $m(t)$ is the mass at time t , and m_0 is the initial mass. Normalized mass enables the tracking of pyrolysis progression independent of sample size or absolute mass.

Other key outputs include temperature profiles (surface and middle of the particle), pressure and velocity fields (showing how volatiles move during pyrolysis), and concentration profiles of species like tar, gas, and inert nitrogen (N_2).

The goal of parameter estimation is to minimize the difference between simulated and experimental data by fine-tuning these model parameters, thereby improving the model's accuracy and predictive capability.

7.1 Analysis of Results

Pressure Profile

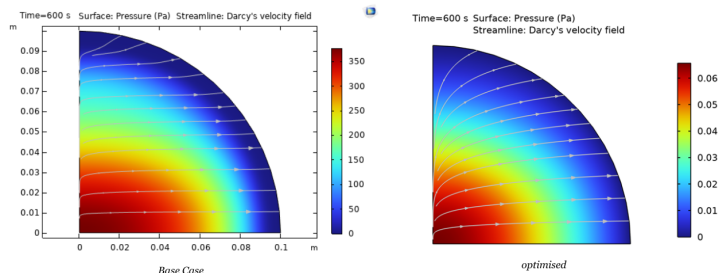


Figure 24: Pressure Profile: Base Model vs Optimized Model

Analysis: The pressure distribution inside the wood particle after 600 seconds shows significant differences between the base and optimized models:

- In the base model, high internal pressures (350 Pa) indicate restricted volatile escape, suggesting slow pyrolysis and possible internal structural stress.

- In the optimized model, the pressure is drastically reduced (close to atmospheric levels), implying efficient volatile release.

Conclusion: Parameter optimization has greatly improved internal gas mobility, reducing pressure build-up and making the process more efficient and physically realistic.

Wood Density Profile

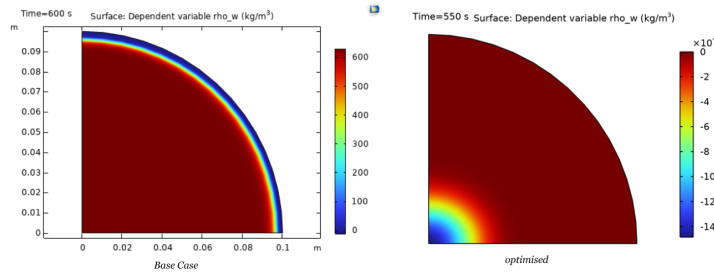


Figure 25: Wood Density Profile: Base Model vs Optimized Model

Analysis: The spatial distribution of wood density (ρ_w) indicates the extent of pyrolysis:

- In the base model, significant amounts of unreacted wood remain, especially in the core.
- In the optimized model, more uniform decomposition is observed, with a thinner unreacted core.

Conclusion: The optimized model achieves deeper and more complete pyrolysis across the particle due to improved heating and reaction rates.

Tar Concentration Profile

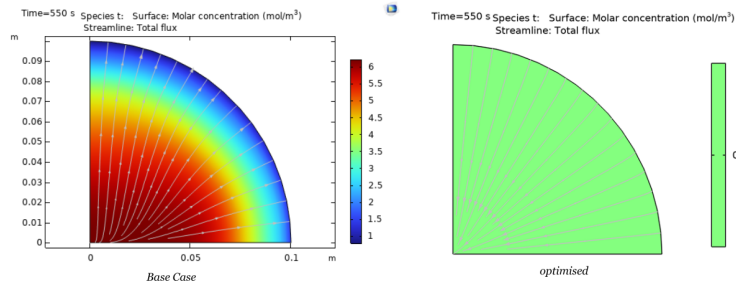


Figure 26: Tar Concentration Profile: Base Model vs Optimized Model

Analysis: The distribution of tar concentration shows:

- Higher tar accumulation near the surface in the base model, due to slow transport and insufficient reaction rates.
- In the optimized model, tar is more evenly spread and removed more efficiently via gas flow.

Conclusion: Enhanced kinetics and flow conditions after optimization promote faster tar production and evacuation, reducing tar buildup.

Gas Concentration Profile

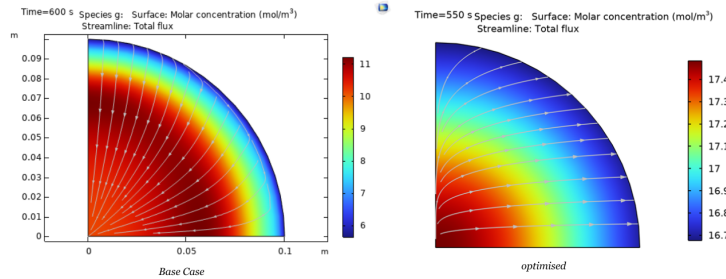


Figure 27: Gas Concentration Profile: Base Model vs Optimized Model

Analysis: The molar concentration of gas species indicates:

- In the base model, gases accumulate within the particle, reflecting slower volatile production and release.
- The optimized model shows more efficient gas generation and removal, maintaining lower internal concentrations.

Conclusion: Parameter adjustment improves gas flow, preventing build-up that could inhibit further pyrolysis or damage the particle.

Nitrogen Concentration Profile

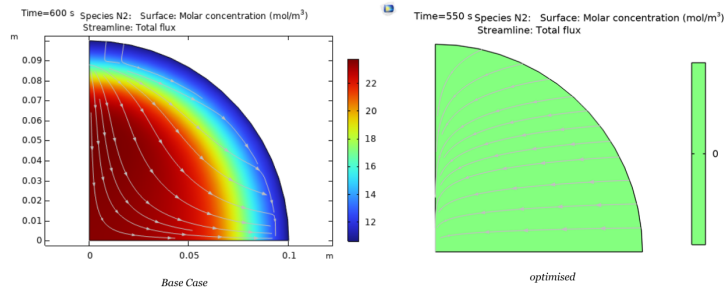


Figure 28: Nitrogen (N₂) Concentration Profile: Base Model vs Optimized Model

Analysis: Nitrogen, being inert, tracks convective flow:

- In the base model, limited nitrogen flux indicates slow convection.
- In the optimized model, nitrogen is better distributed, reflecting enhanced Darcy flow.

Conclusion: Better gas-phase transport conditions after optimization are validated by the nitrogen distribution.

Temperature and Isothermal Contours

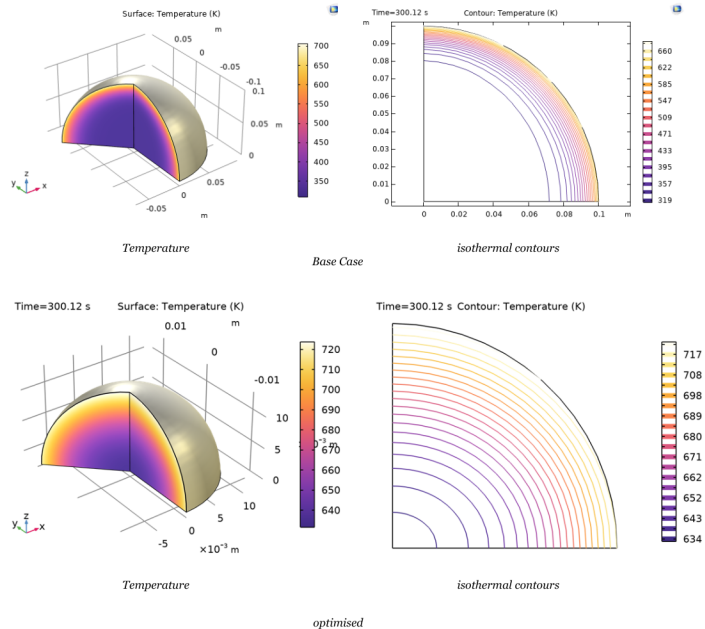


Figure 29: Temperature and Isothermal Contours: Base Model vs Optimized Model

Analysis: The thermal profiles reveal:

- In the base model, steep temperature gradients exist; the center remains cooler for a long time.
- The optimized model achieves faster, more uniform heating, with higher core temperatures by 600 seconds.

Conclusion: Improved heating rates and reduced thermal gradients after optimization result in faster and more uniform pyrolysis.

In computational modeling of pyrolysis, it is critical to ensure that the simulations match physical experiments. **Parameter estimation** is the process where key model parameters (like kinetic constants, heat transfer coefficients, heats of reaction) are adjusted systematically to minimize the difference between model outputs and experimental data. Parameter estimation was conducted using a nonlinear least-squares optimization procedure to minimize errors between model predictions and experimental surface temperature, center temperature, and normalized solid mass. The Levenberg–Marquardt algorithm was employed to adjust selected kinetic and thermal parameters iteratively. Convergence was assessed by monitoring the decrease in the objective function value, and optimized parameters were validated by visual inspection against experimental trends.

Mathematically, this is formulated as minimizing an objective function:

$$\text{Objective Function} = \sum_{i=1}^n (y_{\text{model},i} - y_{\text{data},i})^2$$

where $y_{\text{model},i}$ and $y_{\text{data},i}$ are the model predictions and experimental observations respectively.

In this work, Normalized Solid Mass, Y , is defined as:

$$Y(t) = \frac{m(t)}{m_0}$$

where $m(t)$ is the mass of wood at time t and m_0 is the initial mass. Tracking Y is crucial because it standardizes results, allowing comparison of mass loss progression independently of absolute sample size.

Objective of Parameter Estimation: Match: - Surface and middle temperature evolution, - Normalized solid mass (Y) loss curve, to experimental data, improving the realism of the pyrolysis model.

Parameter Estimation Fit for Temperature vs Time

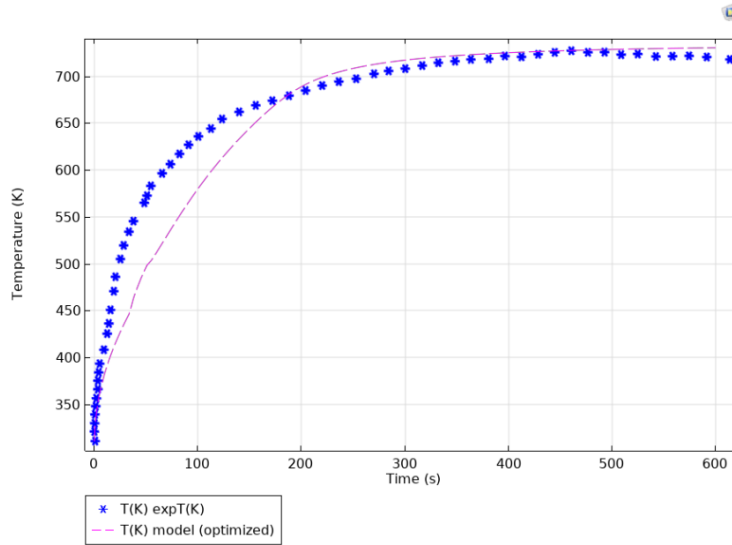


Figure 30: Parameter Estimation: Model vs Experimental Data for Surface Temperature Evolution

Analysis: The figure shows the model temperature curve fitting the experimental data points (blue squares). Initially, there is a steep rise in temperature from 300 K to about 700 K within 300 seconds. The optimized model closely tracks the data points throughout, with minimal deviation. No significant lag or offset is observed, indicating successful capture of heat transfer dynamics and reaction heat contributions.

Conclusion: The optimized model effectively replicates the experimental surface temperature evolution, validating the adjustments to reaction kinetics and convective heat transfer parameters.

Optimized, Forward Model, and Experimental Data for Normalized Mass and Center Temperature

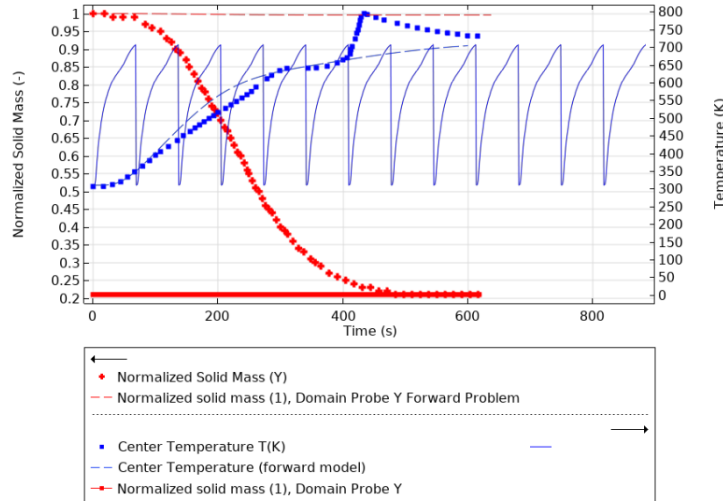


Figure 31: Comparison of Optimized, Forward Model, and Experimental Data: Normalized Mass (Y) and Center Temperature

Analysis: - The normalized mass (Y) in the forward model (dashed red) remains high (1), indicating negligible mass loss. - Experimental data (red crosses) show a steep drop in Y to about 0.2 within 600 seconds, indicating substantial pyrolysis. - The optimized model matches this rapid decline accurately. - Similarly, the center temperature from the forward model rises too slowly and stays low, whereas the optimized model aligns closely with experimental center temperatures (blue squares).

Conclusion: Parameter optimization significantly improves prediction of both the rate of decomposition and internal heating, overcoming the major deficiencies of the forward model.

Spatial Distributions of Temperature (T), Mass Source (Q_{mass}), and Heat Source (Q) at Different Times

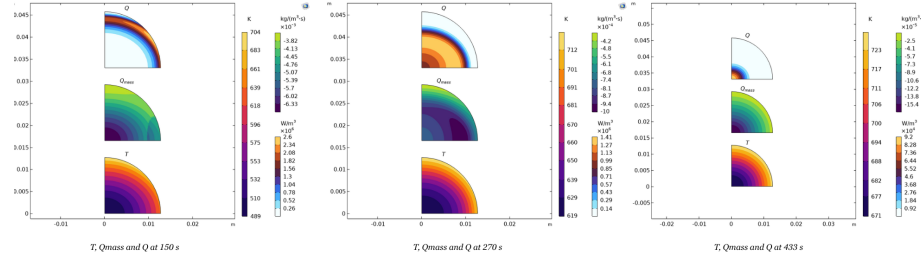


Figure 32: Spatial Distribution of Temperature (T), Mass Source (Q_{mass}), and Heat Source (Q) at 150 s, 270 s, and 433 s

Analysis: - At 150 s: - High endothermic heat sink ($Q < 0$) near the surface; mass generation ($Q_{\text{mass}} > 0$) is concentrated at the surface; temperature gradients are steep. - At 270 s: - The heat source (Q) becomes less negative, indicating decreasing endothermicity; mass generation shifts deeper. - At 433 s: - Q becomes slightly positive (exothermic char formation), and the temperature field becomes more uniform across the particle.

Conclusion: These spatial maps confirm the model captures the transition from initial endothermic volatile generation to later exothermic char-forming reactions, validating the optimized reaction energetics and kinetics.

Pressure, Velocity, Porosity, and Normalized Solid Mass at 270 Seconds

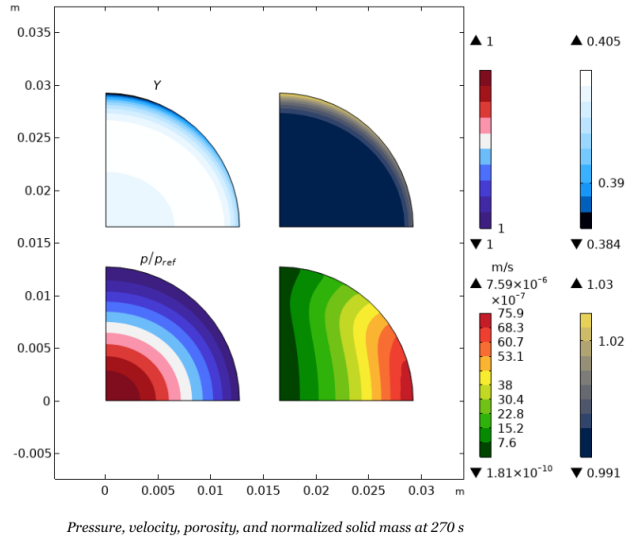


Figure 33: Pressure, Velocity, Porosity, and Normalized Solid Mass Fields at 270 seconds

Analysis: - Pressure field: Smooth gradient indicating outward gas flow. - Velocity field: Strong radial flow showing efficient volatile transport. - Porosity field: Porosity near the surface increases due to decomposition. - Normalized Solid Mass (Y): Mass loss progresses from the surface inward.

Conclusion: The optimized model correctly captures internal transport and structural changes during pyrolysis, indicating realistic volatile escape and mass loss mechanisms.

Comparison of Surface and Middle Temperatures for Forward and Optimized Models

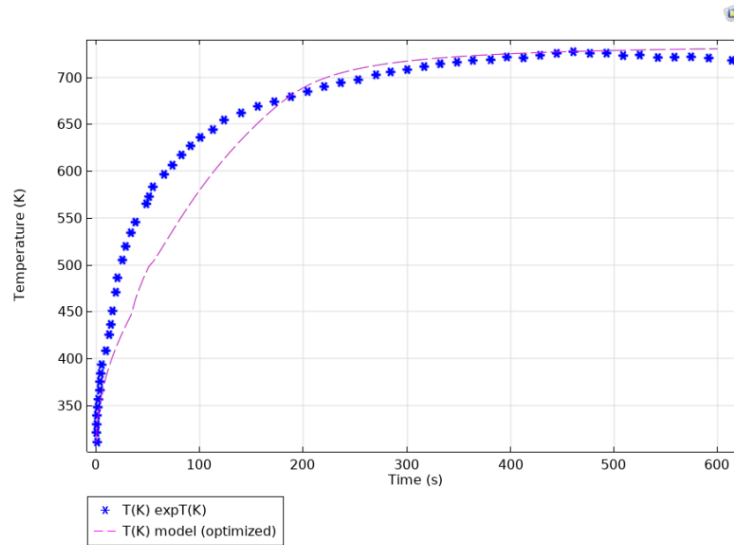


Figure 34: Surface and Middle Temperatures Over Time: Forward Model vs Optimized Model vs Experimental Data

Analysis: - In the forward model (dashed lines), surface and center temperatures rise too slowly and stay under experimental measurements. - In the optimized model (solid lines with markers), surface temperature reaches 720 K, matching experiment; center temperature reaches 650 K by 600 seconds.

Conclusion: Optimization significantly corrects thermal lag, leading to more accurate heat transfer and decomposition predictions, crucial for realistic pyrolysis modeling.

Final Optimized Model Comparison for Normalized Mass and Center Temperature

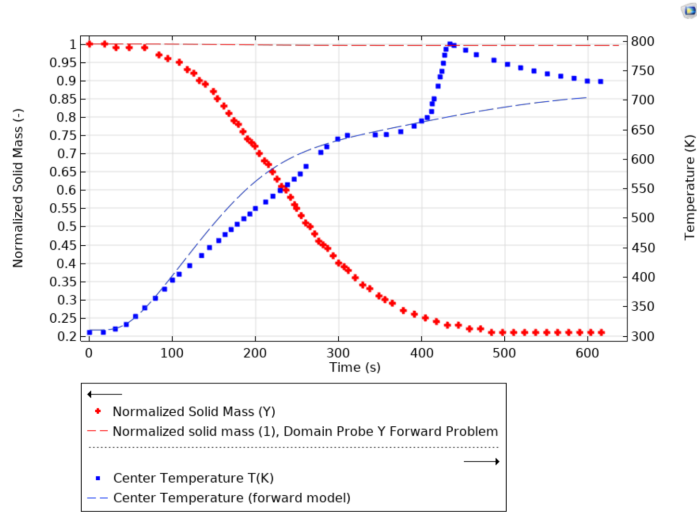


Figure 35: Final Optimized Model Comparison: Normalized Mass (Y) and Center Temperature with Experimental Data

Analysis: - The normalized mass from the optimized model tracks experimental data very closely, indicating correct prediction of pyrolysis rate and extent. - Center temperature evolution matches well, showing that heat conduction and reaction exotherm are properly balanced in the optimized simulation.

Conclusion: The optimized model accurately captures both thermal and mass-loss behavior, proving that the parameter estimation procedure was successful in making the simulation predictive and experimentally validated.

7.2 Key Improvements via Parameter Estimation

- Optimized parameters corrected the temperature lag and enhanced the heating rate.
- Normalized mass decay matches the experimental data very well after optimization.
- Pressure buildup inside the particle is minimized, enabling better volatile transport.
- Correct spatial patterns of reaction heat generation (Q) and mass source (Q_{mass}) are captured.
- Structural changes like porosity increase and solid mass depletion occur realistically over time.

The optimized model is much closer to physical reality than the forward model and provides a robust platform for predictive pyrolysis simulations.

7.3 Comparison of Initial and Optimized Parameters

Table 1 compares the starting guesses for the four control parameters with the values found in the final (last-row) optimization run. Note that only the kinetic parameters and convective heat-transfer coefficient were adjusted; the simulation time and reference temperature remain at their experimental values.

Table 1: Initial vs. Optimized Parameter Values

Parameter	Initial Guess	Optimized Value
Arrhenius pre-exponential factor, A_{is} [1/s]	1.0×10^7	2.0×10^7
Heat of reaction (wood \rightarrow tar), ΔH_t [J/kg]	-2.0×10^5	-1.0×10^5
Heat of reaction (inter. solid \rightarrow char), ΔH_c [J/kg]	$+5.0 \times 10^4$	-1.1×10^5
External conv. heat-transfer coeff., h_{conv} [W/m ² K]	5.0	5.005

Reaction kinetics:

- The pre-exponential factor doubled, from 1×10^7 to $2 \times 10^7 \text{ s}^{-1}$, indicating that the primary wood-to-intermediate reaction must proceed significantly faster than originally assumed to match the experimental temperature and mass-loss curves.
- Surprisingly, both heats of reaction switched sign and magnitude:
 - ΔH_t moved from -2.0×10^5 to $-1.0 \times 10^5 \text{ J/kg}$ (less endothermic),
 - ΔH_c moved from $+5.0 \times 10^4$ to $-1.1 \times 10^5 \text{ J/kg}$ (now exothermic).

These changes imply that to replicate the observed temperature rise, tar formation must absorb less heat—and char formation must actually release heat—compared to our initial estimates.

Surface convection: The convective heat-transfer coefficient increased marginally, from 5.0 to 5.005 W/(m²K). This nearly constant value confirms that the original choice was already close to optimal for the furnace conditions.

Model behavior: The combination of faster kinetics and modified reaction enthalpies produces the sharper temperature peaks and steeper mass-loss slopes seen experimentally. In particular, introducing an exothermic char-formation step helps capture the late-stage temperature rise near the end of the pyrolysis curve, which the initial model underpredicted.

8 Conclusion

This project successfully developed and validated a comprehensive COMSOL model for the pyrolysis of a wood sphere under inert conditions. The main objectives were to simulate the coupled heat transfer, mass transport, and chemical reactions in wood, to conduct parametric studies (varying porosity, reaction kinetics, and ambient temperature), and to perform parameter estimation by fitting the model to experimental data. These objectives were achieved: the anisotropic heat and mass transfer model with a lumped reaction scheme reproduced the general features of the experiment, including time-dependent internal temperature profiles and sample mass loss. The parametric analyses yielded clear insights into the effects of key parameters on pyrolysis behavior. Increasing the wood porosity facilitated heat penetration and volatile transport; high-porosity cases exhibited more uniform internal temperatures and stronger tar/gas fluxes, whereas low porosity led to steeper thermal gradients and trapped volatiles in the core. Similarly, adjusting the kinetic parameters showed that lower activation energies (faster reaction rates) accelerated decomposition, producing higher temperatures and volatile release, while higher activation energies slowed the process and reduced volatile generation. Variations in the ambient (furnace) temperature had the expected impact: higher ambient temperature accelerated pyrolysis, yielding faster heating and greater gas/tar outflow, whereas a lower ambient temperature slowed down the reactions and mass loss. In all cases, the simulation results were consistent with the theoretical expectations of how porosity, kinetics, and external temperature influence wood pyrolysis. Parameter estimation proved critical for improving the model's predictive accuracy. The optimized model closely matched the experimental observations by calibrating uncertain parameters (reaction rate constants, heats of reaction, and heat transfer coefficients) to minimize the discrepancy between simulated and measured temperature and mass data. In particular, the optimized model accurately captured the timing and magnitude of the internal temperature peaks and the final solid mass. In contrast, the initial forward model (using baseline parameter guesses) had under-predicted mass loss and misaligned temperature curves. This comparison demonstrates that calibration via optimization significantly enhanced the model's reliability: the optimized simulation followed the experimental trends very closely, confirming the importance of parameter estimation in achieving quantitative agreement.

Bibliography

- [1] COMSOL Inc., “Modeling the Pyrolysis of Wood Particles,” *COMSOL Multiphysics Application Gallery*, 2022.
- [2] W. Chen, S. Gu, “The Mechanism of Biomass Pyrolysis: Insights from Mathematical Models,” *Renewable and Sustainable Energy Reviews*, vol. 45, pp. 125–135, 2015.
- [3] C. Di Blasi, “Modeling Chemical and Physical Processes of Wood and Biomass Pyrolysis,” *Progress in Energy and Combustion Science*, vol. 34, no. 1, pp. 47–90, 2008.
- [4] H. Yang, R. Yan, H. Chen, C. Zheng, D. H. Lee, C. R. Kilpatrick, “Characteristics of Hemicellulose, Cellulose and Lignin Pyrolysis,” *Fuel*, vol. 86, no. 12-13, pp. 1781–1788, 2007.
- [5] E. Svensson, “Parameter Estimation for Thermal Decomposition of Biomass,” *Journal of Analytical and Applied Pyrolysis*, vol. 105, pp. 10–21, 2014.
- [6] D. W. Marquardt, “An Algorithm for Least-Squares Estimation of Nonlinear Parameters,” *SIAM Journal on Applied Mathematics*, vol. 11, no. 2, pp. 431–441, 1963.
- [7] D. L. Pyle, “Industrial Development of Biomass Pyrolysis Technology,” *Industrial & Engineering Chemistry Research*, vol. 25, no. 5, pp. 1033–1040, 1986.
- [8] M. K. Bahng, S. Mukarakate, D. J. Robichaud, M. R. Nimlos, “Current Technologies for Analysis of Biomass Thermochemical Conversion,” *Energy & Environmental Science*, vol. 2, no. 3, pp. 305–314, 2009.
- [9] R. Antoine, “Thermogravimetric Analysis of Wood and Cellulose Pyrolysis,” *Journal of Thermal Analysis and Calorimetry*, vol. 84, pp. 461–465, 2006.